Journal of Molecular Spectroscopy 355 (2019) 8–13

Contents lists available at ScienceDirect

Journal of Molecular Spectroscopy

journal homepage: www.elsevier.com/locate/jms

Sub-Doppler rovibrational spectroscopy of the ν_1 fundamental band of D_2H^+

Charles R. Markus [a], Philip A. Kocheril [a], Benjamin J. McCall [a,b,*]

[a] Department of Chemistry, University of Illinois, Urbana, IL 61801, USA
[b] Department of Astronomy, University of Illinois, Urbana, IL 61801, USA

ARTICLE INFO

Article history:
Received 14 September 2018
In revised form 3 November 2018
Accepted 7 November 2018
Available online 09 November 2018

Keywords:
Molecular ion
Rovibrational spectroscopy
Sub-Doppler spectroscopy
High-precision spectroscopy
D_2H^+

ABSTRACT

The molecular ion D_2H^+ is an important species in cold interstellar environments and a key benchmark for *ab initio* calculations. We have measured 37 transitions in the ν_1 fundamental band using the sub-Doppler technique Noise Immune Cavity Enhanced Optical Heterodyne Velocity Modulation Spectroscopy. Using an optical frequency comb for accurate frequency calibration, the uncertainties for most transitions were improved by more than an order of magnitude. These new measurements lead to improved predictions of pure rotational transition frequencies which have not been observed by THz observatories or laboratory spectrometers.

1. Introduction

H_3^+ and its isotopologues are the simplest polyatomic molecules, and their experimentally determined energy levels act as valuable benchmarks for cutting-edge *ab initio* theory [1]. Calculations which go beyond the Born–Oppenheimer approximation with corrections for adiabatic, non-adiabatic, and relativistic effects should be of similar quality for all isotopologues, making H_2D^+ and D_2H^+ of particular importance for investigations of H_3^+ [2].

H_3^+ also plays a central role in the chemistry of molecular clouds, where it is generated by cosmic ray ionization of H_2 and initiates a chain of ion–neutral reactions [3,4]. Despite the estimated low galactic D/H ratio of 2.3×10^{-5} [5], deuterium fractionation leads to significant abundances of D_2H^+ in cold and shielded regions such as dense molecular clouds and prestellar cores [6]. The first astronomical observation of D_2H^+ was of its $1_{10} \rightarrow 1_{01}$ rotational transition in a prestellar core. It was found to be in similar abundance to H_2D^+, which helped confirm new models of deuterium chemistry [7]. The $1_{11} \leftarrow 0_{00}$ transition has since been observed with the German REceiver for Astronomy at Terahertz frequencies (GREAT) on board the airborne Stratospheric Observatory For Infrared Astronomy (SOFIA), where the *ortho* to *para* ratio of D_2H^+ helped determine the age of the prestellar core [8]. The $3_{22} - 3_{13}$ and $4_{13} - 4_{04}$ transitions near 2.5 THz are within the coverage of GREAT, and their predicted frequencies have uncertainties of 5–15 MHz [9]. However, the energies of the 3_{13} and 4_{04} states are 200 cm^{-1} (288 K) and 316 cm^{-1} (454 K) respectively, and to have sufficient population for an observation the rotational temperature would need to be higher than that of a dense molecular cloud. If an event caused the cloud to be warmed after D_2H^+ was generated, such as the formation of a protostar, observations of these transitions could become feasible.

To date, there have been seven pure rotational transitions of D_2H^+ measured in either extended negative glow discharges or cold ion traps [10–13]. The remaining THz transitions must be inferred indirectly using rovibrational data via combination differences (CDs) or spectroscopic constants by fitting to an effective Hamiltonian. So far, 10 rovibrational transitions have been measured with sub-MHz uncertainties by laser induced reaction spectroscopy [14]. The remaining data from multipass absorption experiments have estimated uncertainties of 60 MHz [15,16]. To obtain MHz-level uncertainty on calculated THz transitions, more extensive rovibrational data are needed.

Here, we report the measurement of 37 rovibrational transitions of D_2H^+ in the ν_1 fundamental band using the technique Noise Immune Cavity Enhanced Optical Heterodyne Velocity Modulation Spectroscopy (NICE-OHVMS) [17]. Of these, 10 had never been observed and 17 had their uncertainties reduced from

* Corresponding author at: Department of Chemistry, University of Illinois, Urbana, IL 61801, USA.
E-mail address: bjmccall@illinois.edu (B.J. McCall).
URL: http://www.bjm.scs.illinois.edu (B.J. McCall).

https://doi.org/10.1016/j.jms.2018.11.005
0022-2852/

60 MHz to 2 MHz. Using CDs and a fit to an Euler Hamiltonian [18], improved predictions of unobserved THz transitions are provided.

2. Methods

In order to precisely determine the rest frequencies of rovibrational transitions, measurements must overcome Doppler broadening which can be on the order of several 100 MHz. Sub-Doppler spectroscopy uses counter-propagating beams to generate a Lamb dip centered at the rest frequency, where the width is determined instead by the much smaller homogeneous broadening. Sub-Doppler spectroscopy of molecular ions in laboratory plasmas is challenging given that ions have large collisional cross sections, which significantly increases the homogeneous broadening. In addition, ions are generated in low abundances requiring sensitive spectroscopic techniques. The technique Noise-Immune Cavity-Enhanced Optical Heterodyne Molecular Spectroscopy (NICE-OHMS) is highly sensitive and can generate a large amount of intracavity power which is beneficial for sub-Doppler spectroscopy [19]. However, NICE-OHMS can suffer from background signals due to parasitic etalons and residual amplitude modulation [20], and to mitigate these we have implemented velocity modulation [21] as an additional layer of modulation in the combined technique NICE-OHVMS [17].

All measurements were obtained using our NICE-OHVMS instrument, which has been described previously [22]. In brief, ~1 W of tunable mid-infrared (mid-IR) light from an optical parametric oscillator (OPO, Aculight Argos 2400 SF) is locked to an external cavity (finesse ~150) using a Pound–Drever–Hall scheme. A fiber-coupled elecro-optic modulator phase modulates the pump laser of the OPO at a frequency equal to the free spectral range of the cavity (77 MHz). This allows for the FM sidebands used for heterodyne detection to be generated on the mid-IR idler beam and coupled into cavity modes adjacent to the carrier. The cavity surrounds a triple-jacketed positive column discharge cell, "Black Widow" [23]. Ions are generated by flowing a 2:1 mixture of D_2:H_2 through the cell at 470 mTorr of total pressure, and electrodes at the ends of the cell are driven by a 50 kHz 2 kV peak-to-peak sinusoidal voltage from a step-up transformer. The ions are cooled by flowing either liquid nitrogen or chilled water around the inner cell, achieving rotational temperatures of 170 and 600 K respectively. A CaF_2 window is used to pick off 500 μW of the light transmitted from the cavity, which is focused onto a fast mid-IR thermoelectrically cooled MCT detector (VIGO PVI-4TE-6). The signal is first demodulated by a pair of RF mixers referenced to the heterodyne modulation frequency, and a 90° delay cable is used to obtain the in-phase (dispersion) and quadrature (absorption) signals. The outputs of the mixers are further demodulated by a pair of lock-in amplifiers referenced to twice the discharge frequency (100 kHz) to recover the velocity modulation signal.

Accurate frequency calibration of the idler is accomplished by measuring the difference between the pump and signal frequencies of the OPO using a GPS-referenced optical frequency comb (Menlo Systems FC-1500, 100 MHz repetition rate). The integer difference in comb modes is determined using a mid-IR wavemeter, and the signal beam is locked at a 20 MHz offset to the nearest comb tooth using a phase-locked loop. The frequency is scanned by stepping the pump frequency in 2 MHz increments, and a double-pass acousto-optic modulator (AOM) keeps the beat between the pump and the nearest comb tooth within a bandpass centered at 30 MHz using a feed-forward scheme [24]. When the AOM reaches the end of its diffraction efficiency, it jumps 100 MHz to the next comb tooth. With this, the idler frequency can be determined to within 100 kHz.

3. Results

An example NICE-OHVMS scan of the $2_{11} \leftarrow 2_{02}$ transition of the ν_1 fundamental band of D_2H^+ can be seen in Fig. 1. The detection angle can be set such that the dispersion (in-phase) and absorption (quadrature) components of the signal are separated. The overall odd lineshape is the Doppler profile, and the narrower feature at the center is a set of Lamb dips separated by half-integer multiples of our heterodyne frequency centered around the line center. The homogeneous broadening is approximately 70 MHz, causing these features to overlap. The sub-Doppler feature is fit using Lorentzian functions for the Lamb dips and the Doppler profile is fit with a cubic function centered at the line center, which is shown in Fig. 2. By fitting all channels simultaneously, the line center can be determined as described by Hodges et al. [22].

When we measured 5 scans of the $2_{21} \leftarrow 1_{10}$ transition we found a standard deviation of 300 kHz, but when we compared this to Jusko et al. [14] we found it was in error by 3.1 MHz. Similar results were found with other transitions. First, we confirmed that

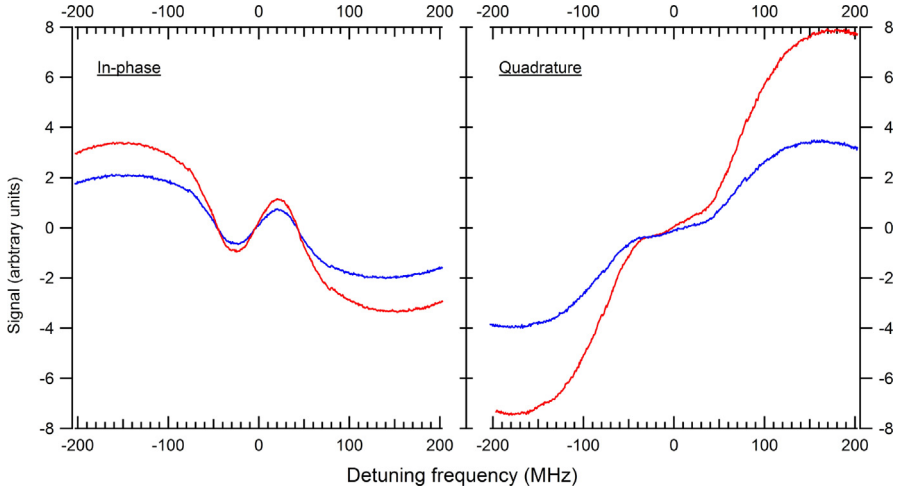

Fig. 1. A NICE-OHVMS scan of the $2_{11} \leftarrow 2_{02}$ transition of the ν_1 fundamental band of D_2H^+, with the frequency offset by 83035089.34 MHz for clarity. The left plot displays the in-phase channels with respect to heterodyne detection, while the right plot displays the quadrature signals. The red and blue traces represent the in-phase and quadrature components of velocity modulation respectively. (For interpretation of the references to color in this figure legend, the reader is referred to the web version of this article.)

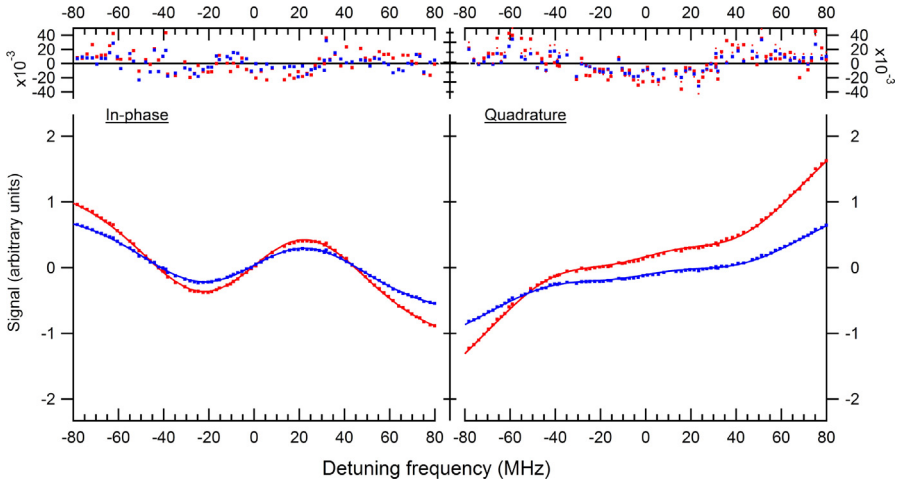

Fig. 2. The sub-Doppler feature of a NICE-OHVMS scan of the $2_{11} \leftarrow 2_{02}$ transition of the ν_1 fundamental band of D_2H^+, with the frequency offset by 83035089.34 MHz for clarity. The points represent the data and solid traces represent the fit, with the residuals shown above. The left plot displays the in-phase channels with respect to heterodyne detection, while the right plot displays the quadrature signals. The red and blue traces represent the in-phase and quadrature components of velocity modulation respectively. (For interpretation of the references to color in this figure legend, the reader is referred to the web version of this article.)

the source of the error was not our frequency calibration using sub-Doppler measurements of methane with a double-pass experiment [24]. Ultimately, we found that small adjustments to the alignment to our cavity would cause one of the lobes of the Doppler profile to be diminished, giving the appearance of the Lamb dip being nearer to the top or bottom of the Doppler profile. This caused a shift in the frequency from the fit and structure to appear in the residuals due to the Doppler profile not being centered around the Lamb dips. The asymmetries in the Doppler profile persisted when the heterodyne modulation was removed for scans using cavity-enhanced velocity modulation spectroscopy, and without velocity modulation in Noise-Immune Cavity-Enhanced Optical Heterodyne Molecular Spectroscopy (NICE-OHMS) scans of methane.

This turned out to be useful, as the NICE-OHMS scans of methane could be used to quantify the asymmetry. The Doppler profile of methane transitions were fit to a NICE-OHMS lineshape with an asymmetry parameter. The angle of injection was adjusted until the asymmetry was eliminated, and then scans of D_2H^+ were collected with the same alignment. The D_2H^+ Lamb dips would then appear centered on the Doppler profile, improving the quality of the fits. This reduced the discrepancy with the values reported by Jusko et al. to within 1.05 MHz. We were also able to compare energy level spacings determined by CDs with highly accurate rotational data, in which all agreed within 1.9 MHz.

Using methane to set the alignment before each set of scans, we measured 37 transitions in the ν_1 fundamental band. The line center frequencies, which are the average of two sets of 4–5 scans taken on two separate days, are listed in Table 1 with comparisons to previous values. The uncertainty for each transition is reported as 2 MHz or the standard deviation of all scans, whichever is larger. Of these 37 transitions, 10 had never been previously observed and 17 were only known to within 60 MHz.

4. Discussion

The new rovibrational transition frequencies can predict pure rotational transitions either through CDs or a fit to an effective Hamiltonian. CDs in the ground state are determined by taking the difference between two transitions that share a final state. These CDs can then be combined with known rotational frequencies to predict unobserved transitions. Our new measurements lead to 20 ground state CDs, which are presented in Table 2 along with CDs determined by Jusko et al. [14] and comparisons to spacings calculated from THz data [11,10,13]. Ten unobserved rotational transitions can be predicted from these CDs with uncertainties of approximately 3 MHz, which are presented in Table 4. In cases where a rotational transition could be calculated in different ways, multiple frequencies are listed.

Frequencies predicted by CDs are trustworthy in that they do not rely on fitting to a model Hamiltonian, whereas predictions from molecular constants will depend on how extensive the initial data set was, and what particular parameters were included in the fit. However, molecular constants can predict a larger set of transitions and can have improved uncertainties when even a limited number of transitions measured with microwave accuracy are included in the fit. Therefore, we also included a fit to an effective Hamiltonian and used the frequencies predicted by CDs as a validation.

D_2H^+ is a "floppy" molecule, which leads to large centrifugal distortion at excited rotational levels. This causes parameters in a Watson-type Hamiltonian to have oscillatory behavior, especially for the series of N_z^{2n} coefficients. This leads to poor convergence unless a large number of terms are included. For this reason we opted to use an Euler Hamiltonian using the method developed by Pickett et al. [18], which Jusko et al. [10] successfully used to fit the ground state of D_2H^+. It has also been successfully used to fit other molecules which have large centrifugal distortion such as D_2O and CH_2 to high rotational levels [25,26]. The standard angular momentum operators N_i^2 and $\mathbf{N}^2$ are replaced by the Euler functions N_i^{2*} and $\mathbf{N}^{2*}$ which are defined as:

$$N_i^{2*} = \frac{N_i^2}{1 + aN_z^2 + b(\mathbf{N}^2 - N_z^2)} \tag{1}$$

$$\mathbf{N}^{2*} = \frac{\mathbf{N}^2 - N_z^2}{1 + aN_z^2 + b(\mathbf{N}^2 - N_z^2)} \tag{2}$$

where the coefficients a and b are chosen transformation parameters. The subscript i represents the rotational axis a, b, or c, and in the I^r representation $a = z, b = x$, and $c = y$. The Euler expansion of the Hamiltonian is then:

$$\mathcal{H}_{rot}^E = \sum_{i,j} X_{ij} (N_a^{2*})^i (\mathbf{N}^{2*})^j + \sum_{i,j} \frac{1}{2} Y_{ij} \{ (N_a^{2*})^i (\mathbf{N}^{2*})^j, N_b^{2*} - N_c^{2*} \} \tag{3}$$

Table 1
Transition frequencies of the v_1 fundamental band from this work with residuals (O–C) from the fit and comparisons with previous studies. The 1σ uncertainties are given in parentheses.

Transition	This work (MHz)	O–C (MHz)	Prev. Value (MHz)	Diff.	Ref.
$2_{11} \leftarrow 3_{22}$	77590937.46(200)	−2.92	–		
$1_{10} \leftarrow 2_{21}$	78389394.87(200)	−1.93	–		
$3_{13} \leftarrow 4_{04}$	78509936.60(200)	−3.39	–		
$2_{02} \leftarrow 3_{13}$	79070989.38(200)	−0.94	79070980(60)	9.38	[15]
$2_{12} \leftarrow 3_{03}$	79433535.00(200)	−1.53	–		
$4_{04} \leftarrow 4_{13}$	79446380.39(211)	4.13	–		
$3_{13} \leftarrow 3_{22}$	79481913.99(200)	1.04	–		
$1_{01} \leftarrow 2_{12}$	79782520.69(200)	1.22	79782508(60)	12.69	[15]
$2_{12} \leftarrow 2_{21}$	79941256.46(200)	−2.73	–		
$1_{11} \leftarrow 2_{02}$	80452752.63(200)	0.98	80452751.59(75)	1.04	[14]
$0_{00} \leftarrow 1_{11}$	80575855.74(200)	0.24	80575855.46(12)	0.28	[14]
$3_{12} \leftarrow 3_{21}$	80615629.64(200)	1.62	–		
$2_{11} \leftarrow 2_{20}$	80626375.46(200)	0.15	–		
$1_{01} \leftarrow 1_{10}$	81349548.28(200)	−0.01	81349548.38(15)	−0.10	[14]
$1_{10} \leftarrow 1_{01}$	82713780.02(200)	−0.35	82713780.40(15)	−0.37	[14]
$2_{11} \leftarrow 2_{02}$	83035089.34(200)	−0.83	83035106(60)	−16.66	[15]
$3_{21} \leftarrow 3_{12}$	83258225.69(200)	−1.71	83258242(60)	−16.31	[15]
$2_{20} \leftarrow 2_{11}$	83319483.33(200)	−1.51	83319459(60)	24.33	[15]
$1_{11} \leftarrow 0_{00}$	83502180.44(200)	−0.65	83502181.08(90)	−0.64	[14]
$2_{02} \leftarrow 1_{11}$	83591104.21(200)	0.29	83591103.84(15)	0.37	[14]
$3_{12} \leftarrow 3_{03}$	83611788.86(200)	−0.24	83611817(60)	−28.14	[15]
$2_{21} \leftarrow 2_{12}$	84014925.65(200)	0.21	84014926.35(78)	−0.69	[14]
$2_{12} \leftarrow 1_{01}$	84265643.03(200)	0.26	84265642.81(12)	0.22	[14]
$3_{30} \leftarrow 3_{21}$	84277356.85(200)	0.65	–		
$4_{13} \leftarrow 4_{04}$	84400948.70(223)	0.19	84400990(60)	−41.30	[15]
$3_{22} \leftarrow 3_{13}$	84414871.55(200)	−0.33	84414901(60)	−29.45	[15]
$3_{03} \leftarrow 2_{12}$	84558339.15(200)	0.71	84558381(60)	−41.85	[15]
$3_{13} \leftarrow 2_{02}$	84926063.15(200)	0.41	84926047(60)	16.22	[15]
$4_{04} \leftarrow 3_{13}$	85412859.83(200)	−3.15	85412850(60)	9.83	[15]
$4_{14} \leftarrow 3_{03}$	85573374.36(200)	0.32	85573389(60)	−14.64	[15]
$2_{21} \leftarrow 1_{10}$	85581954.85(200)	0.57	85581954.15(18)	0.70	[14]
$2_{20} \leftarrow 1_{11}$	85930971.82(200)	0.12	85930971.78(15)	0.04	[14]
$5_{05} \leftarrow 4_{14}$	86188742.45(200)	1.36	86188773(60)	−30.55	[15]
$5_{15} \leftarrow 4_{04}$	86248883.92(200)	−1.79	86248911(60)	−27.08	[15]
$3_{22} \leftarrow 2_{11}$	86323498.28(200)	−0.31	86323499(60)	−0.72	[15]
$3_{21} \leftarrow 2_{12}$	87486539.30(346)	−0.83	87486574(60)	−34.70	[15]
$3_{30} \leftarrow 2_{21}$	87781239.63(200)	−0.31	87781240(60)	−0.37	[15]

Table 2
List of ground state CDs derived from measurements of the v_1 fundamental band with comparison to values calculated from THz measurements. The 1σ uncertainties are given in parentheses.

CD	Frequency (MHz)	From THz data (MHz)	Diff. (MHz)
$3_{03} - 2_{21}$	507721.46(283)	–	–
$4_{04} - 3_{22}$	971977.39(283)	–	–
$2_{12} - 1_{10}$	1567027.58(283)	–	–
$2_{12} - 1_{10}$	1567029.20(283)	–	–
$2_{12} - 1_{10}$	1567027.80(80) [14]	–	–
$3_{13} - 2_{11}$	1908626.74(283)	1908626.71(10) [11,10]	0.03
$2_{20} - 2_{02}$	2408713.89(283)	2408714.74(30) [10,13]	−0.85
$2_{11} - 1_{11}$	2611488.49(283)	2611486.86(10) [11,10]	1.63
$3_{21} - 3_{03}$	2996159.22(283)	2996161.11(14) [11]	−1.89
$3_{22} - 2_{20}$	3035437.99(283)	–	–
$2_{02} - 0_{00}$	3049427.81(283)	3049429.43(10) [11,10]	−1.62
$2_{02} - 0_{00}$	3049427.49(76) [14]	3049429.43(10) [11,10]	−1.94
$3_{21} - 2_{21}$	3503882.79(283)	–	–
$3_{12} - 2_{12}$	4228313.61(283)	–	–
$2_{21} - 1_{01}$	4324385.16(283)	–	–
$2_{21} - 1_{01}$	4324386.57(283)	–	–
$3_{13} - 1_{11}$	4520114.84(283)	4520113.57(14) [11]	1.27
$3_{03} - 1_{01}$	4832108.03(283)	–	–
$3_{22} - 2_{02}$	5444149.16(283)	–	–
$3_{22} - 2_{02}$	5444151.88(283)	–	–
$4_{13} - 3_{13}$	5966479.44(291)	–	–
$4_{04} - 2_{02}$	6431252.66(283)	–	–

where $\{,\}$ is the anticommutator and X_{ij} and Y_{ij} are the diagonal and off-diagonal spectroscopic parameters, respectively. It should be noted that the a and b transformation parameters need not be the same for different vibrational states, or for the diagonal and off-diagonal parts of the expansion [18].

For our two-state fit, the ground state parameters were initially held to the values determined by Jusko et al. [10], and initial guesses for a and b parameters for $v_1 = 1$ were calculated from the Watson-type parameters [18]. First, CDs from rovibrational studies of the v_2 and v_3 fundamental bands and pure rotational data were included [16,11,10,27,13]. Then, rovibrational transitions from this work and Lubic & Amano [15] were added sequentially in order of increasing final K_a. When the root-mean-square (RMS) error grew large, the term which was found to reduce the

Table 3
Spectroscopic parameters from a two-state fit of the v_1 fundamental band to an Euler Hamiltonian. All values are in MHz. The 1σ uncertainties are given in parentheses.

Parameter	Ground	$v_1 = 1$
$a_x \times 10^3$	2.5	1.2
$b_x \times 10^3$	0.48	0.37
$a_y \times 10^3$	7.3	12
$b_y \times 10^3$	1.5	1.6
v_0	–	82052461.194(114)
X_{01}	1085199.67(51)	1062119.165(237)
X_{10}	523757.577(120)	518150.388(130)
X_{20}	1893.84(65)	413.410(82)
X_{11}	1409.674(115)	719.762(176)
X_{02}	79.0888(254)	9.7879(293)
X_{30}	4.239(126)	1.0551(84)
X_{21}	0.8502(139)	−1.4353(233)
X_{12}	2.0071(153)	1.3862(147)
X_{03}	0.05467(54)	0.08293(94)
Y_{00}	65984.820(134)	65141.907(162)
Y_{10}	28.279(114)	311.871(121)
Y_{01}	33.9370(74)	36.0269(66)

Table 4
Comparison of predicted rotational frequencies from CDs, molecular constants, and CDMS [9]. All values are in MHz. The 1σ uncertainties are given in parentheses.

Transition	From CDs	From molecular constants	From CDMS
$2_{21} \leftarrow 2_{12}$	2065696.17(400)	2065694.313(420)	2065690.46(283)
–	2065696.91(294)	–	–
–	2065698.32(294)	–	–
$3_{12} \leftarrow 2_{21}$	2162617.23(283)	2162618.406(809)	2162613.00(714)
–	2162617.45(283)	–	–
$2_{12} \leftarrow 1_{01}$	2258688.24(80)	2258689.259(273)	2258688.25(77)
$3_{22} \leftarrow 3_{13}$[a]	2496859.31(283)	2496859.93(142)	2496835.9(154)
–	2496862.03(283)	–	–
–	2496862.89(285)	–	–
$4_{13} \leftarrow 4_{04}$[a]	2497642.74(400)	2497653.56(145)	2497660.95(507)
$3_{03} \leftarrow 2_{12}$	2573417.84(283)	2573416.977(578)	2573407.69(506)
–	2573419.78(294)	–	–
$4_{04} \leftarrow 3_{13}$	3468836.70(283)	3468833.17(165)	3468810.1(192)
$4_{13} \leftarrow 3_{22}$	3469616.55(401)	3469626.80(213)	3469635.2(277)
$2_{21} \leftarrow 1_{10}$	3632724.71(283)	3632723.129(416)	3632718.28(303)
–	3632726.12(283)	–	–
$3_{22} \leftarrow 2_{11}$	4405486.02(283)	4405486.65(142)	4405462.6(154)
–	4405488.74(283)	–	–
–	4405489.59(284)	–	–
$3_{21} \leftarrow 2_{12}$	5569578.95(283)	5569578.058(590)	5569568.80(507)

[a] Within coverage of the SOFIA GREAT instrument.

error the most was included. When the transitions $4_{23} \leftarrow 4_{14}$ and $6_{06} \leftarrow 5_{15}$ were included, we found that their assignments by Lubic & Amano [15] needed to be switched. Once all transitions were added, 12 total rotational parameters were used in the $v_1 = 1$ excited state. Then, all X_{ij} and Y_{ij} parameters for both states were allowed to float and the transformation parameters a_X, b_X, a_Y, and b_Y were then adjusted one at a time to obtain the best fit result. Overall, 25 parameters were used to fit 49 states from 121 transitions and CDs. A reduced RMS error of 0.72 was obtained for all data and 0.71 for our data alone. The files from the fit are included in the supplementary material. In comparison, a fit to a traditional two-state Watson-type Hamiltonian with 25 parameters resulted in a reduced RMS error of 2.2, and required an additional 8 parameters to reach a reduced RMS error below 1 of 0.60.

The resulting parameters from the fit are in Table 3, and the residuals from the fit are listed in Table 1. Calculated rotational transition frequencies are listed in Table 4 along with comparisons to predictions from CDs and the Cologne Database for Molecular Spectroscopy (CDMS) [9]. Predictions from the newly determined molecular constants have improved upon the uncertainties of previous values by at least a factor of 2, and in most cases by a factor of ~10. The two transitions which fall within the coverage of the SOFIA GREAT instrument, $3_{22} \leftarrow 3_{13}$ and $4_{13} \leftarrow 4_{04}$, had their uncertainties improved from 15.4 and 5.07 MHz to 1.42 and 1.45 MHz respectively.

Table 5
Watson-type molecular constants calculated from the Euler-type parameters determined by the fit, with comparison to Watson-type parameters determined by Yu et al. [11].

Ground parameter	Converted	Previous work [11]
A	1085199.67(51)	1085216.75(175)
B	655727.217(293)	655655.2(24)
C	391787.937(292)	391847.91(168)
Δ_K	570.85(66)	569.29(182)
Δ_{JK}	75.99(13)	89.01(135)
Δ_J	172.315(25)	169.580(183)
δ_K	388.37(11)	354.91(92)
δ_J	65.0402(74)	63.509(79)
Φ_K	5.36(13)	4.98(40)
Φ_{KJ}	−5.371(37)	−3.82(43)
Φ_{JK}	1.465(16)	1.367(167)
Φ_J	0.0993(6)	0.0[a]

[a] Fixed.

The Euler-type parameters can be converted to Watson-type parameters for comparison by expanding the denominators of N_i^{2*} and $\mathbf{N}^{2*}$ in Eq. (3) and gathering terms of the correct order [18]. The converted Watson parameters are presented in Table 5 and compared to previous works. The ground state molecular constants are generally in agreement with those determined by Yu et al. Many parameters do disagree outisde of their respective uncertainties, however molecular constants for "floppy" molecules can vary widly depending on the particular line list and parameter set used [10]. A comparison of the converted $v_1 = 1$ parameters with those from Lubic & Amano [15] was omitted, since the switched assignment of the $4_{23} \leftarrow 4_{14}$ and $6_{06} \leftarrow 5_{15}$ transitions caused their parameters to be significantly off.

5. Conclusion

In this work, we have greatly expanded the number of rovibrational transitions of D_2H^+ measured with MHz-level uncertainty from 10 to 37 using the sub-Doppler technique NICE-OHVMS. These values have been used to predict unobserved rotational transitions using molecular constants from a fit to an Euler Hamiltonian. The uncertainties of the predicted frequencies, including two within the coverage of the SOFIA GREAT instrument, have been significantly reduced to approximately 1.5 MHz. These frequencies will also assist in laboratory searches for unobserved THz transitions. Moreover, these new measurements will act as valuable benchmarks for *ab intio* calculations which go beyond the Born–Oppenheimer approximation.

Acknowledgments

C.R.M. is grateful for support from the National Aeronautics and Space Administration Earth and Space Science Fellowship (NESSF NNX16AO86H). P.A.K. is grateful for funding from the University of Illinois at Urbana-Champaign Undergraduate Summer Research Scholarship, and for financial support from a Peter C. & Gretchen Miller Markunas Scholarship and a Matthews Scholarship. This work was also funded by the National Science Foundation (NSF

PHY 14-04330). We also acknowledge Holger S.P. Müller for helpful discussions regarding the Euler Hamiltonian.

Appendix A. Supplementary material

Supplementary data associated with this article can be found, in the online version, at https://doi.org/10.1016/j.jms.2018.11.005.

References

[1] J. Tennyson, J. Chem. Phys. 145 (2016) 120901, https://doi.org/10.1063/1.4962907.
[2] M. Pavanello, L. Adamowicz, A. Alijah, N.F. Zobov, I.I. Mizus, O.L. Polyansky, J. Tennyson, T. Szidarovszky, A.G. Császár, J. Chem. Phys. 136 (2012) 184303, https://doi.org/10.1063/1.4711756.
[3] E. Herbst, W. Klemperer, Astrophys. J. 185 (1973) 505–533, https://doi.org/10.1086/152436.
[4] W.D. Watson, Astrophys. J. 183 (1973) L17, https://doi.org/10.1086/181242.
[5] J.L. Linsky, B.T. Draine, H.W. Moos, E.B. Jenkins, B.E. Wood, C. Oliveira, W.P. Blair, S.D. Friedman, C. Gry, D. Knauth, J.W. Kruk, S. Lacour, N. Lehner, S. Redfield, J.M. Shull, G. Sonneborn, G.M. Williger, Astrophys. J. 647 (2006) 1106–1124, https://doi.org/10.1086/505556.
[6] H. Roberts, E. Herbst, T.J. Millar, Astron. Astrophys. 424 (2004) 905–917, https://doi.org/10.1051/0004-6361:20040441.
[7] C. Vastel, T.G. Phillips, H. Yoshida, Astrophys. J. 606 (2004) L127–L130, https://doi.org/10.1086/421265.
[8] J. Harju, O. Sipilä, S. Brünken, S. Schlemmer, P. Caselli, M. Juvela, K.M. Menten, J. Stutzki, O. Asvany, T. Kamiński, Y. Okada, R. Higgins, Astrophys. J. 840 (2017) 63, https://doi.org/10.3847/1538-4357/aa6c69.
[9] H.S.P. Müller, F. Schlöder, J. Stutzki, G. Winnewisser, J. Mol. Struct. 742 (2005) 215–227, https://doi.org/10.1016/j.molstruc.2005.01.027.
[10] P. Jusko, M. Töpfer, H.S.P. Müller, P.N. Ghosh, S. Schlemmer, O. Asvany, J. Mol. Spectrosc. 332 (2017) 33–37, https://doi.org/10.1016/j.jms.2016.09.013.
[11] S. Yu, J. Pearson, T. Amano, F. Matsushima, J. Mol. Spectrosc. 551 (2012) 6–8, https://doi.org/10.1016/j.jms.2016.10.012.
[12] O.L. Polyansky, A.R.W. McKellar, J. Chem. Phys. 92 (1990) 4039, https://doi.org/10.1063/1.457817.
[13] D. Jennings, C. Demuynck, M. Banek, K. Evenson, personal communication, cited by Polyansky & McKellar, 1990.
[14] P. Jusko, C. Konietzko, S. Schlemmer, O. Asvany, J. Mol. Spectrosc. 319 (2016) 55–58, https://doi.org/10.1016/j.jms.2015.12.002.
[15] K.G. Lubic, T. Amano, Can. J. Phys. 62 (1984) 1886–1888, https://doi.org/10.1139/p84-232.
[16] S.C. Foster, A.R.W. McKellar, J.K.G. Watson, J. Chem. Phys. 85 (1986) 664, https://doi.org/10.1063/1.451841.
[17] B.M. Siller, M.W. Porambo, A.A. Mills, B.J. McCall, Opt. Exp. 19 (2011) 24822–24827, https://doi.org/10.1364/OE.19.024822.
[18] H.M. Pickett, J.C. Pearson, C.E. Miller, J. Mol. Spectrosc. 233 (2005) 174–179, https://doi.org/10.1016/j.jms.2005.06.013.
[19] J. Ye, L.-S. Ma, J.L. Hall, J. Opt. Soc. Am. B 15 (1998) 6, https://doi.org/10.1364/JOSAB.15.000006.
[20] A. Foltynowicz, I. Silander, O. Axner, J. Opt. Soc. Am. B 28 (2011) 2797, https://doi.org/10.1364/JOSAB.28.002797.
[21] C.S. Gudeman, M.H. Begemann, J. Pfaff, R.J. Saykally, J. Chem. Phys. 78 (1983) 5837, https://doi.org/10.1063/1.445428.
[22] J.N. Hodges, A.J. Perry, P.A. Jenkins II, B.M. Siller, B.J. McCall, J. Chem. Phys. 139 (2013) 164201, https://doi.org/10.1063/1.4825251.
[23] B.J. McCall, Spectroscopy of H_3^+ Laboratory and Astrophysical Plasmas Ph.D. thesis, University of Chicago, 2001.
[24] P.A. Kocheril, C.R. Markus, A.M. Esposito, A.W. Schrader, T.S. Dieter, B.J. McCall, J. Quant. Spectrosc. Radiat. Transf. 215 (2018) 9–12, https://doi.org/10.1016/j.jqsrt.2018.04.033.
[25] S. Brünken, H.S.P. Müller, C. Endres, F. Lewen, T. Giesen, B. Drouin, J.C. Pearson, H. Mäder, PCCP 9 (2007) 2103–2112, https://doi.org/10.1039/B613925F.
[26] S. Brünken, H.S.P. Müller, F. Lewen, T.F. Giesen, J. Chem. Phys. 123 (2005), https://doi.org/10.1063/1.2074467.
[27] T. Hirao, T. Amano, Astronom. J. 597 (2003) L85, https://doi.org/10.1086/379801.